Article

Vibration Characteristics Analysis of Immersed Tunnel Structures Based on a Viscoelastic Beam Model Embedded in a Fluid-Saturated Soil System Due to a Moving Load

Hongyuan Huang [1,2,3], Yao Rong [4], Xiao Xiao [1,3] and Bin Xu [1,3,*]

1 Department of Civil Engineering, Nanchang Institute of Technology, Nanchang 330029, China; 18970836454@163.com (H.H.)
2 Key Laboratory of Hydraulic and Waterway Engineering of the Ministry of Education, Chongqing Jiaotong University, Chongqing 400074, China
3 Jiangxi Provincial Engineering Research Center of the Special Reinforcement and Safety Monitoring Technology in Hydraulic & Civil Engineering, Nanchang 330099, China
4 Jiangxi Transportation Research Institute, Nanchang 330200, China
* Correspondence: xmq418@163.com

Abstract: This study aims to investigate the vibration responses on underwater immersed tunnels caused by moving loads, taking into account factors such as the viscoelastic characteristics of riverbed water, foundation soil, and the immersed tunnel itself. An ideal fluid medium is adopted to simulate the water, while a saturated porous medium is used to simulate the riverbed soil layer. The immersed tunnel structure is simplified as an infinitely long viscoelastic Euler beam, and the vibration effects are described by the theory of the standard linear solid model, taking into account structural damping. The coupled dynamic control equations were established by utilizing the displacement and stress conditions at the interface between the ideal fluid medium, the saturated porous medium, and the immersed tunnel structure. The equivalent stiffness of the riverbed water and site foundation was obtained. Furthermore, the numerical solutions of the tunnel displacement, internal forces, and pore pressure in the riverbed site were obtained in the time-space domain using the IFFT (Inverse Fast Fourier Transform) algorithm. The correctness of the model was validated by comparing the results with existing studies. The numerical results show that the riverbed water significantly reduces the Rayleigh wave velocity of the immersed tunnel structure in the riverbed-foundation system. Therefore, it is necessary to control the driving speed during high water levels. As the permeability of the saturated riverbed foundation increases, the vertical displacement, bending moment, and shear force of the beam in the immersed tunnel structure will increase. As the viscosity coefficient of the viscoelastic beam in the immersed tunnel structure increases, the vertical vibration amplitude of the beam will decrease, but further increasing the viscosity coefficient of the beam will have little effect on its vibration amplitude. Therefore, the standard solid model of the viscoelastic beam can effectively describe the creep and relaxation phenomena of materials and can objectively reflect the working conditions of the concrete structure of the immersed tunnel.

Keywords: underwater immersed tunnel; viscoelastic Euler beam; moving load; Helmholtz acoustic equation; IFFT algorithm

1. Introduction

Different from bridges, immersed tunnels have their own unique advantages and have become an important method for crossing rivers and seas. It has become one of the key engineering projects for controlling the modern urban transportation network. Compared to other types of underground structures, immersed tunnels have a lighter weight, which could cause anti-floating problems. However, monitoring of existing projects has shown that immersed tunnels experience varying degrees of settlement during operation [1,2].

For example, the 1646 m long Fort McHenry Tunnel in the United States has a maximum settlement of 162 mm, and the Shanghai Outer Ring immersed tunnel has a maximum settlement of 310 mm. As a special type of underground building, the prediction of the stress, deformation, and riverbed settlement of an immersed tunnel caused by train operation has become a hot topic in civil engineering.

Currently, the main methods for analyzing the structural dynamic response and foundation settlement of underwater immersed tunnels during operation are indoor experiments, on-site monitoring, theoretical calculations, and numerical analysis. Such as Grantz [1,3] The multiple causes of the settlement of the immersed tunnel were summarized, and the theory was verified by multiple tunnel monitoring data sets. Schmidt et al. [4] monitored the settlement of the Second Hampton Roads Tunnel from the construction period to the operation period, and the results showed that the immersed tunnel on the soft soil foundation had a large settlement. Based on the long-term health monitoring of the large diameter tunnel in Hangzhou, Shiming Wu et al. [5] summarized the rules of the reinforcement internal force, the interface pressure, and the settlement of the tunnel and analyzed the reasons when the long-term upper load changes and the short-term tide level were large. Considering the underwater immersed tunnel was greatly influenced by the surrounding medium, the dynamic characteristic analysis process was more complex; simplification is generally performed. The underwater immersed tunnel structure is supported by a continuous beam on an elastic foundation or joint using spring simulation, and soil-structure interaction is simulated using spring and damping to simulate multiple particle systems, such as wei gang, etc. [6] introduced the Kelvin viscoelastic simple-supported Euler beam model into the dynamic analysis of the submarine immersed tunnel and obtained the dynamic analytical solution of the displacement, bending moment, and ground reaction force of the immersed tunnel under the action of a vehicle load. Peak et al. [7] obtained the maximum reaction value of the train load to the foundation of the immersed tunnel by the influence line method. Wei Gang et al. [8] modified the elastic foundation beam method for calculating the vertical settlement of an immersed tunnel, proposed a method of calculating the foundation soil settlement using the rebound modulus of the soil body, and calculated the vertical settlement of an immersed tunnel in normal and limiting conditions, respectively. In recent years, numerical analysis has been widely applied in related fields. Zhou et al. [9] used a combination of model tests and numerical simulations, based on time-domain and frequency-domain analysis, to study the response of excess pore water pressure and the vertical acceleration response of shield tunnel structures under train vibration loads. Yang et al. [10] used numerical simulation to study the dynamic response of tunnel structures as well as the attenuation characteristics of vibration waves in the stratum based on time-frequency analysis. In documents [11–13] the seismic design analysis of immersed tunnels was carried out using the response displacement method of a multi-particle system and the mass-spring model method.

The structure of submerged tube tunnels is typically composed of concrete and polymer composites. Under external loads, it exhibits not only elastic deformation, which demonstrates the characteristics of an elastic solid, but also viscous deformation, which demonstrates the characteristics of a viscous material. This means that it can generate damping during the energy dissipation process. Therefore, submerged tube tunnels can be classified as viscoelastic materials. Viscoelastic damping materials play a significant role in controlling structural vibrations, and the analysis of vibration problems related to these materials is receiving more attention from experts and scholars. Gu et al. [14] and Liu, etc. [15] analyzed the constitutive relation of viscoelastic materials using statics experiments, derived the constitutive equation of viscoelastic materials in the complex number domain, time domain, and frequency domain, respectively, and studied the dissipation energy of viscoelastic damping materials. Surie & Cederbaum [16] proposed constitutive equations for viscoelastic materials based on the Boltzmann principle and studied analytically the basic kinetic model of nonlinear elastic beams. Argyris, etc. [17] analyzed the chaotic motion of viscoelastic beams by using the constitutive relation of

diffeomorphic viscoelastic materials. Liqun Chen et al. [18,19] established the partial differential-integral equation of the nonlinear viscoelastic moving beam to illustrate the dynamic mathematical model of the geometric nonlinear viscoelastic beam and simplified the equation. Marynowski & Kapitaniak [20] analyzed the dynamic properties of stable moving beams by exploiting the viscoelastic constitutive relation of the viscoelastic model. Junqiang Li [21] further discussed several typical models, such as the complex modulus model, fraction and exponential model, fraction and derivative model, and microoscillator model, and their dynamic applications according to the research on constitutive equations of linear viscoelastic materials in recent years. Li Biao et al. [22] analyzed the amplitude and frequency response of the control model of a nonlinear viscoelastic Timoshenko beam, which affects the stability of the structure, and analyzed the influence of damping and external effects of viscoelastic materials on the stable state of the structure applying the numerical simulation method. The aforementioned research results indicate that neglecting the viscoelastic damping characteristics of structural materials will affect the accuracy of structural vibration analysis.

In conclusion, there is currently a significant amount of research regarding the dynamic response of submarine pipelines and river-crossing tunnel structures to loads such as earthquakes and waves. However, there is relatively limited research on the dynamic response of submerged tube structures caused by moving loads. In order to study the submerged tube tunnel, the load-structure model was adopted to calculate the internal forces, deformations, and settlements of the tube sections. Various factors are converted into static loads applied to the structure, and the foundation is assumed to be a Winkler foundation. The cross-section is analyzed as a plane truss structure, and the longitudinal direction is simulated as an elastic foundation beam. This method has several assumptions and notable drawbacks. For instance, it ignores the settlement deformation of the foundation and the time factor of settlements, resulting in the settlement calculation value being much smaller than the measured value. Due to deformation compatibility, the settlement of the foundation and foundation soil will lead to the redistribution of internal forces in the immersed tunnel, which may result in significant stress or displacement and damage to the pipe sections and joints. Furthermore, using finite element or other numerical analysis software to handle the semi-infinite space problem of the foundation in submerged tube tunnels requires a large number of calculation elements, which can be difficult to implement. Although it is possible to use artificial boundaries and establish various transmission boundary models for analysis, there are problems such as insufficient accuracy in low-order boundaries and poor stability in high-order boundaries.

Therefore, an ideal fluid medium is adopted to simulate the water layer, while a saturated porous medium is used to simulate the riverbed soil layer. The underwater tunnel structure is simplified as an infinitely long viscoelastic Euler beam, and the vibration effects are described by the theory of the standard linear solid model, taking into account structural damping. The coupled dynamic control equations were established by utilizing the displacement and stress conditions at the interface between the ideal fluid medium, the saturated porous medium, and the underwater tunnel structure. The equivalent stiffness of the riverbed water and site foundation was obtained. Furthermore, the numerical solutions of the tunnel structure's vibration displacement, internal forces, and pore pressure in the riverbed site were obtained in the time-space domain using the IFFT algorithm. Using the calculation model proposed in this article, the influence of different factors on the dynamic response of underwater, immersed tunnel structures under moving loads was analyzed.

2. The Simplified Calculation Model and Control Equation of an Underwater Immersed Tunnel

A simplified two-dimensional physical model is adopted for the underwater immersed tunnel, as shown in Figure 1, and the water depth of the river bed is h_w, the buried depth of the underwater tunnel is H, h_s from the river bed bedrock, the load concentration is Fz, the velocity of the vertical mobile load is v_c, considering the coupling of the riverbed water

and riverbed foundation and underwater immersed tunnel, riverbed water using ideal fluid media, riverbed foundation layer using saturated porous medium theory simulation, underwater immersed tunnel structure simplified to infinite long viscoelastic Euler beam, using the standard linear solid model theory, describing the structure damping influence on vibration.
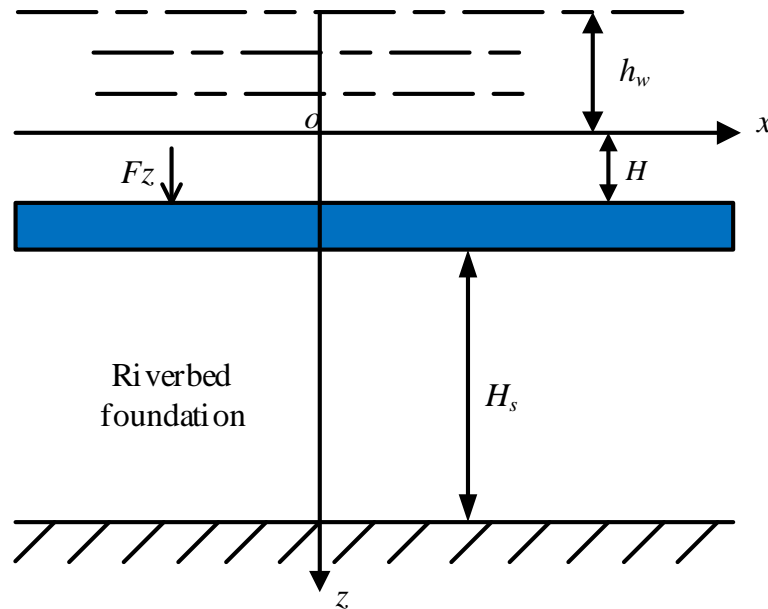
Figure 1. A schematic illustration of the water-soil-viscoelastic beam coupling system under a moving load.

Riverbed water is a theoretical fluid, and the dynamic control equation uses Helmholtz's acoustic equation [23]:

$$\nabla^2 p_{fw} - \frac{1}{v_w^2}\frac{\partial^2 p_{fw}}{\partial t^2} = 4\pi\delta(z - z_s) \tag{1}$$

In the formula: v_w respectively represents the fluid water pressure and the acoustic wave speed in the fluid, z_s indicates the position of the action point of the sound source.

The Biot theory of saturated soil [24] is used for the riverbed foundation description, and the momentum conservation equations of saturated pore medium and pore fluid are, respectively,

$$\begin{aligned}
\mu u_{i,jj} + (\lambda + \alpha^2 M + \mu)u_{j,ii} - \alpha M w_{j,ji} &= (\rho \dot{u}_i + \rho_f \ddot{w}_i)\\
\alpha M u_{j,ji} + M w_{j,ji} &= \rho_f \ddot{u}_i + m \ddot{w}_i + bp \dot{w}_i
\end{aligned} \tag{2a,b}$$

In the formula: u_i, w_i ($i = 1,2$) are the displacements of the soil skeleton and the permeability displacements of the fluid relative to the soil skeleton. The point above the displacement indicates the derivative of time; λ, μ is the Lame constant; α, M are Biot soil skeleton and water compression parameters, respectively; ρ, ρ_f is saturated soil and pore water density; f is porosity; $m = a_\infty \rho_f / f$, a_∞ is the bending coefficient of the pore medium; bp represents the amount related to the viscosity of the pore fluid and the permeability coefficient of the soil.

The constitutive equations for saturated soil and pore water are, respectively.

$$\begin{aligned}
\sigma_{ij} &= \lambda e \delta_{ij} + \mu(u_{i,j} + u_{j,i}) - \alpha \delta_{ij} p\\
p &= -\alpha M e + M\theta
\end{aligned} \tag{3a,b}$$

In the formula: $e = u_{i,j}$, $\theta = -w_{i,j}$ is the incremental quantity of volumetric strain of the soil skeleton and the fluid volume in the unit volume pore medium, respectively; σ_{ij}, p is the total stress component and pore water pressure, respectively.

The rectangular underwater immersed tunnel with a cross section shown in Figure 2 is simplified to an infinitely long viscoelastic Euler beam according to the paper [25,26] method, and the vibration equation is as follows:

$$\rho_B \ddot{W}_b + E_b I_b \frac{\partial^4 W_b}{\partial x^4} = Fz\delta(x - v_c t)$$
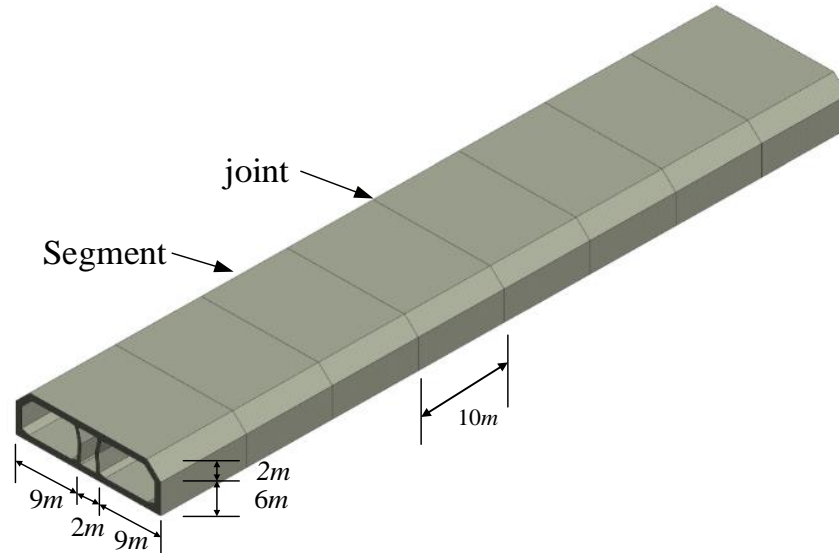$$+ a(\sigma_{zz}(x, h^-, t) - \sigma_{zz}(x, h^+, t)) \tag{4}$$

Figure 2. Schematic diagram of the immersed tunnel structure.

In the formula: E_b, ρ_B, $W_b I_b$ are the structure density, vertical displacement, and tube section stiffness of the immersed tunnel, respectively; Fz is the load amplitude; and a is the equivalent average diameter of the cross-section of the underwater immersed tunnel.

For the infinitely long viscoelastic Euler beam, the standard linear solid model theory is used to describe its damping situation, and the compound elastic modulus of the viscoelastic beam is:

$$E_b = E_{bR}\left(\frac{1 + i\omega\tau_{b\varepsilon}}{1 + i\omega\tau_{b\sigma}}\right), \ E_{bR} = \frac{E_b^{(1)} E_b^{(2)}}{E_b^{(1)} + E_b^{(2)}}$$

$$\tau_{b\sigma} = \frac{\eta}{E_b^{(1)} + E_b^{(2)}}, \ \tau_{b\varepsilon} = \frac{\eta}{E_b^{(2)}} \tag{5}$$

In the formula: $E_b^{(1)}$ and $E_b^{(2)}$ is the elastic parameter of the viscoelastic beam in the standard solid model; η is the viscosity coefficient.

Considering the riverbed surface ($z = 0$) impervious condition, there are the following boundary conditions:

$$\left.\begin{array}{l} u_{wz}(x, z = 0, t) = u_z(x, z = 0, t) \\ p_{fw}(x, z = 0, t) = -\sigma_{zz}(x, z = 0, t) \\ \sigma_{zx}(x, z = 0, t) = 0 \\ w_z(x, z = 0, t) = 0 \end{array}\right\} \tag{6}$$

Considering the riverbed surface ($z = 0$) permeability, the following boundary conditions are provided:

$$\left.\begin{array}{l} u_{wz}(x, z = 0, t) = u_z(x, z = 0, t) + w_z(x, z = 0, t) \\ p_{fw}(x, z = 0, t) = p(x, z = 0, t) \\ \sigma_{zx}(x, z = 0, t) = 0 \\ \sigma_{zz}(x, z = 0, t) = -p_{fw}(x, z = 0, t) \end{array}\right\} \tag{7}$$

At the riverbed water surface of ($z = -h_w$), there are:

$$p_{fw}(x, z = -h_w, t) = 0$$

If the displacement of the tunnel is zero in the horizontal direction and there is continuous displacement between the tunnel structure and the soil layer in the vertical direction, the following boundary conditions are provided:

$$u_x(x, H^-, t) = u_x(x, H^+, t) = 0,$$
$$w_z(x, H^-, t) = w_z(x, H^+, t) = W_b(x, t) \tag{8}$$

For bottom bedrock, the following displacement boundary conditions are provided:

$$u_z(x, z = H + Hs, t) = w_z(x, H + Hs, t) = 0. \tag{9}$$

3. The Frequency Domain and Wave Number Domain Solutions and the Equivalent Stiffness

The decoupling method is used to solve the Biot equation by adopting a potential function to represent each displacement component in the soil, and the displacement vectors U and W can be expressed by four potential functions Φ, Ψ, χ, and φ.

$$U = \nabla\phi + \nabla \times \psi; \quad W = \nabla\chi + \nabla \times \varphi \tag{10a,b}$$

By substituting the Equation (10a,b) into the Biot control Equation (2a,b), two decoupled equations can be obtained.

$$\left. \begin{array}{l} [K_p][L]\{\ddot{\phi}\} = [N]\{\phi\} + [R]\{\dot{\phi}\} \\ [K_s][L]\{\ddot{\psi}\} = [N]\{\psi\} + [R]\{\dot{\psi}\} \end{array} \right\} \tag{11a,b}$$

In formula:

$$[K_p] = \begin{bmatrix} \lambda + \alpha^2 M + 2G & \alpha M \\ \alpha M & M \end{bmatrix}$$

$$[K_s] = \begin{bmatrix} G & 0 \\ 0 & 0 \end{bmatrix} [L] = \begin{bmatrix} \nabla^2 & 0 \\ 0 & \nabla^2 \end{bmatrix}$$

$$[N] = \begin{bmatrix} \rho & \rho_f \\ \rho_f & m \end{bmatrix} [R] = \begin{bmatrix} 0 & 0 \\ 0 & b \end{bmatrix}$$

Two-dimensional Fourier transformation from space to wavenumber $x \to \xi$, time to frequency, $t \to \omega$

$$\left. \begin{array}{l} \overline{\widetilde{f}}(\xi, \omega) = \int\limits_{-\infty}^{\infty} \int\limits_{-\infty}^{\infty} f(x, t) e^{-i(\xi x + \omega t)} dx dt \\ f(x, t) = \frac{1}{(2\pi)^2} \int\limits_{-\infty}^{\infty} \int\limits_{-\infty}^{\infty} \overline{\widetilde{f}}(\xi, \omega) e^{i(\xi x + \omega t)} d\xi d\omega \end{array} \right\} \tag{12a,b}$$

In formula: Superscript $^{-, \sim}$ represents $x \to \xi$, $t \to \omega$ the value of the two-dimensional Fourier transform domain.

According to the Biggios principle [27], Equation (11a,b) can perform the Helmholtz decomposition:

$$\nabla^2 \widetilde{\phi}_f + r_1^2 \widetilde{\phi}_f = 0 \quad \nabla^2 \widetilde{\phi}_s + r_2^2 \widetilde{\phi}_s = 0 \quad \nabla^2 \widetilde{\psi} + r_3^2 \widetilde{\psi} = 0 \tag{13}$$

In the formula, r_1, r_2, r_3 are the complex wavenumbers of compressed fast, slow, and shear waves, respectively.

In the rectangular coordinate system, the soil skeleton, fluid displacement, stress, and pore pressure can be expressed by the potential function:

$$
\left.\begin{array}{l}
u_x = \dfrac{\partial \phi}{\partial x} - \dfrac{\partial \psi}{\partial z}; u_z = \dfrac{\partial \phi}{\partial z} + \dfrac{\partial \psi}{\partial x} \\[2mm]
w_x = \dfrac{\partial \chi}{\partial x} - \dfrac{\partial \varphi}{\partial z}; w_z = \dfrac{\partial \chi}{\partial z} + \dfrac{\partial \varphi}{\partial x}
\end{array}\right\}
\tag{14a,b}
$$

By substituting the substitution of Equation (14) into Equation (10), the expressions for displacement, stress, and pore pressure in the Fourier transform domain as follows:

$$
\left[i\widetilde{\widetilde{u}}_x \; \widetilde{\widetilde{u}}_z \; \widetilde{\widetilde{w}}_z \; i\widetilde{\widetilde{\sigma}}_{xz} \; \widetilde{\widetilde{\sigma}}_{zz} \; \widetilde{\widetilde{p}} \right]^T =
\begin{bmatrix} \boldsymbol{D}_d & \boldsymbol{D}_u \\ \boldsymbol{S}_d & \boldsymbol{S}_u \end{bmatrix}
\left[\boldsymbol{W}_d(z)^T \; \boldsymbol{W}_u(z)^T \right]
\tag{15a}
$$

In formula: $\begin{aligned} \boldsymbol{W}_d(\xi, z, \omega) &= [be^{-\gamma_1 z} \; de^{-\gamma_2 z} \; fe^{-\gamma_3 z}] \\ \boldsymbol{W}_u(\xi, z, \omega) &= [ae^{\gamma_1 z} \; ce^{\gamma_2 z} \; ee^{\gamma_3 z}] \end{aligned}$

$$
\boldsymbol{D}_u = \begin{bmatrix} -\xi & -\xi & i\gamma_3 \\ \gamma_1 & \gamma_2 & -i\xi \\ \gamma_1\chi_1 & \gamma_2\chi_2 & -i\xi\gamma_3 \end{bmatrix}; \;
\boldsymbol{D}_d = \begin{bmatrix} -\xi & -\xi & -i\gamma_3 \\ \gamma_1 & -\gamma_2 & -i\xi \\ -\gamma_1\chi_1 & -\gamma_2\chi_2 & -i\xi\gamma_3 \end{bmatrix};
$$

$$
\boldsymbol{S}_u = \begin{bmatrix} -2\mu\xi\gamma_1 & -2\mu\gamma_2\xi & i\chi_3 \\ c_1 & c_2 & -2i\mu\xi\gamma_3 \\ a_1 & a_2 & 0 \end{bmatrix}; \;
\boldsymbol{S}_d = \begin{bmatrix} 2\mu\xi\gamma_1 & 2\mu\gamma_2\xi & i\chi_3 \\ c_1 & c_2 & 2i\mu\xi\gamma_3 \\ a_1 & a_2 & 0 \end{bmatrix};
$$

$$
\chi_k = (\alpha + \kappa_k)M(L_k)^2; \; \gamma_k = \sqrt{\xi^2 - L_k^2} \; (k = 1, 2);
$$

$$
c_k = 2\mu\gamma_1^2 - \lambda(L_k)^2 - \alpha\chi_k (k = 1, 2);
$$

$$
\kappa_k = \left[(\lambda + \alpha^2 M + 2\mu)(L_k)^2 - \rho\omega^2\right] / \left[\rho_f\omega^2 - \alpha M(L_k)^2\right] \; (k = 1, 2);
\tag{15b}
$$

$$
\chi_3 = \mu[\xi^2 + (\gamma_3)^2]; \; \kappa_3 = \rho_f\omega^2 / (ib\omega - m\omega^2);
$$

$$
(S)^2 = (\rho_f\kappa_3 + \rho)\omega^2 / \mu; \; \gamma_3 = \sqrt{\xi^2 - (S)^2};
$$

$$
(L_1)^2 = \tfrac{1}{2}(\beta_1 - \sqrt{(\beta_1)^2 - 4\beta_2}); \; (L_2)^2 = \tfrac{1}{2}(\beta_1 + \sqrt{(\beta_1)^2 - 4\beta_2});
$$

$$
\beta_1 = \left[(m\omega^2 - ib\omega)(\lambda + \alpha^2 M + 2\mu) + \rho\omega^2 M - 2\alpha M\rho_f\omega^2\right] / \left[(\lambda + 2\mu)M\right];
$$

$$
\beta_2 = \left[(m\omega^2 - ib\omega)\rho\omega^2 M - \rho_f^2\omega^4\right] / \left[(\lambda + 2\mu)M\right];
$$

For Equation (1), using the Fourier transformation of time and space domains, the pore pressure of the riverbed fluid in the frequency domain and wavenumber domain is:

$$
\frac{\partial^2 p_{fw}}{\partial z^2} + \gamma_w^2 p_{fw} = -2\delta(z - z_s)
\tag{16}
$$

In formula: $\gamma_w = \sqrt{(k_x^2 - k_w^2)}$, $k_w = \omega / v_w$, and to ensure that the compression wave travels vertically along the fluid, $\mathrm{Re}(k_w) \geq 0$.

This can be obtained:

$$
p_{fw} = A_w e^{\gamma_w z} + B_w e^{-\gamma_w z}
\tag{17}
$$

$$
u_{zw} = \frac{1}{\rho_w\omega^2} \frac{\partial p_{fw}}{\partial z} = \frac{\gamma_w}{\rho_w\omega^2}(A_w e^{\gamma_w z} - B_w e^{-\gamma_w z})
\tag{18}
$$

The vibration equation of the Euler beam in the frequency and wave fields is as follows:

$$
(E_b I_b k_x^4 - \rho_B\omega^2)\widetilde{\overline{W}}_b = 2\pi Fz\delta(\omega - k_x v_c) + a(\widetilde{\overline{\sigma}}_{zz}(k_x, h^-, \omega) - \widetilde{\overline{\sigma}}_{zz}(k_x, h^+, \omega))
\tag{19}
$$

4. Example Calculation and Numerical Analysis

The effective stiffness matrix between the reverse force q considering the coupling of the riverbed water and riverbed foundation and the viscoelastic Euler beam displacement w_b is obtained by Formulas (15a,b), (17)–(19). The equivalent stiffness matrix is then inserted into Formulas (15a,b) and (18) to obtain the expressions of riverbed soil displacement, pore pressure, and stress in the frequency field-wave field. According to the above derivation, the variables in the frequency field can be expressed as commonly as:

$$\widetilde{\overline{\Omega}}(\xi, z, \omega) = \widetilde{\overline{\Omega}}^{*}(\xi, z, \omega) F_z \delta(\omega + \xi v_c) \tag{20}$$

The solutions can be obtained in both the time and space domains by applying the double Fourier inverse transformation to the above equation. Considering the nature of the Dirac-δ function, the double inverse Fourier transformation can be reduced to:

$$\Omega(x, z, t) = (\frac{1}{2\pi})^2 F_z \int_{-\infty}^{+\infty} \widetilde{\overline{\Omega}}(\xi, z, -\xi v_c) e^{i\xi(x - v_c t)} d\xi \tag{21}$$

Due to the complex expression of the integrand function, it is difficult to produce the closed-form solution of the Fourier inverse transformation. In this paper, the IFFT method is adopted to complete the Fourier inverse transformation. In addition, because the layered soil adopts the viscoelastic model, there is no branch point or singularity appearing in the integral path of the horizontal wave number ξ because of the soil viscosity force. The number of discrete points of the wave number ξ is $N = 4096$ [23], spatial interval $\Delta x = 0.1$, and the spatial calculation interval $L_x = N\Delta x$.

The vibration characteristics of the immersed tunnel based on the built-in infinite-length viscoelastic beam model of a fluid-saturated soil system under different water depths, load speeds, saturated soil, and viscoelastic beam parameters are investigated. As shown in Figure 1, the concentration degree of the moving point load is F_z, with a constant velocity v_c along the positive direction of the X axis in the fluid-saturated soil system with the built-in infinite length viscoelastic beam. The viscoelastic beam adopts the standard solid model, in which the viscoelastic parameters are $E_p^{(1)}$, $E_p^{(2)}$ and the viscosity coefficient is η. For the convenience of calculation $v_s = \sqrt{\mu/\rho_s}$, displacement, stress, and pore pressure without dimension as: $u* = 2\pi\mu u a_R / F_z$, $M* = M_x/(F_z a_R^2)$, $Q* = Q_x/(F_z a_R^2)$, $p* = p(x,z,t)A/F_z$, in which the reference length $a_R = 1.0$ m.

Example 1: Model validation.

For comparison with the literature results, if the viscoelastic beam $E_p^{(1)} = E_p^{(2)} = 2.010^9$, $\eta = 0.0$ Pa, then the viscoelastic beam is fully elastic. In addition, when the saturated soil parameters α, b_p, M, ρ_f, ϕ, a_∞ are close to 0, the saturated soil can degenerate into elastic soil. A relatively simple two-dimensional model is considered [26], which consists of an elastic layer possessing a small viscosity and a beam located inside the layer. It is assumed that the layer is infinitely long in the horizontal direction, is fixed along the bottom, and has a traction-free surface. Figure 3 shows the depth of the riverbed as $h_w = 0.0$, the buried depth of the tunnel as $H = 7.0$ m, and from the riverbed bedrock, $h_s = 15.0$ m, moving point load as $F_z = 1.0 \times 10^4$ N·m^{-1}, speed $v_c = 30.0$ ms^{-1}, the vertical and horizontal displacement of the riverbed surface observation point A (0.0 m, 0.0 m) changes with time t, and the calculation results of homogeneous elastic soil-beam conditions are given in the literature [26].

From Figure 3, the solution in this paper is almost consistent with the results of the literature [26].

Example 2: influence of different load speeds and river bed depth.

Under the condition of different load speeds ($v_c = 0.2v_s$, $0.5v_s$, $1.2v_s$), the river bed depth $h_w = 0.0$ m, 2.0 m, 4.0 m, 7.0 m, and the buried depth of the underwater tunnel is H = 1.0 m. From the river bed bedrock, $h_s = 15.0$ m, the displacement changes of
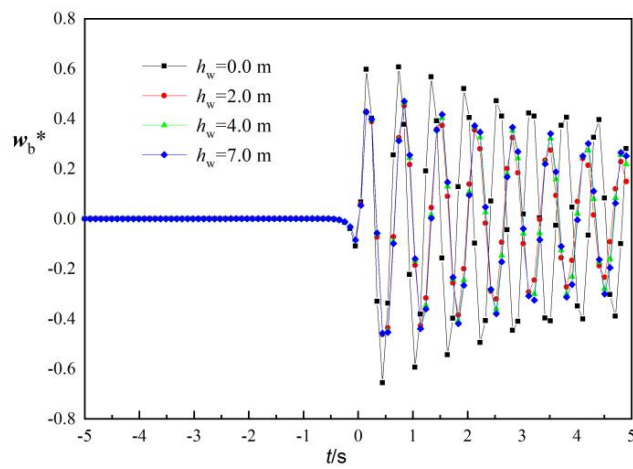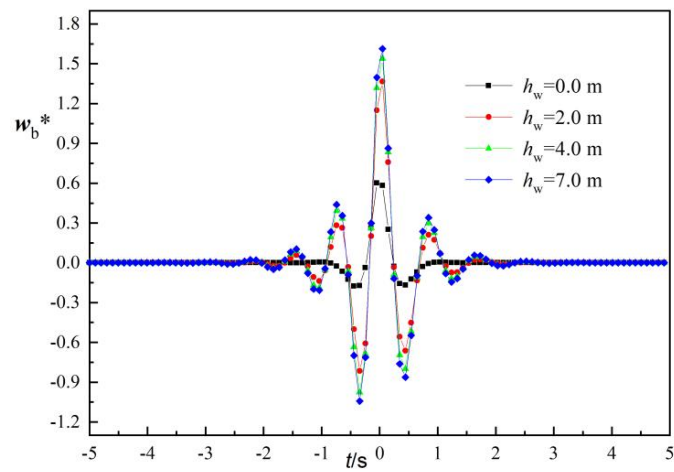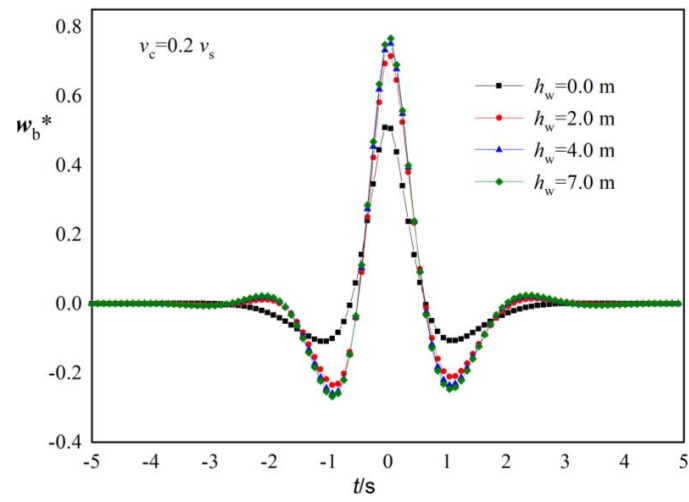
the structural beam of the tunnel are analyzed. As shown in Figure 4, the viscoelastic beam of the underwater immersed tunnel adopts the standard solid model, and the calculated parameters: $E_p^{(1)} = E_p^{(2)} = 2.0 \times 10^9$, $\eta = 3.0 \times 10^5$ Pa, and the calculation parameters of saturated soil and fluid: $\mu = 2.0 \times 10^7$ N/m^2, $\phi = 0.125$, $\lambda = 4.0 \times 10^7$ N/m^2, $\alpha = 0.97$, $M = 2.44 \times 10^8$ N/m^2, $\rho_s = 2.0 \times 10^3$ kg/m^3, $m = 1890$ kg/m^3, $v_w = 1414$ m/s, $b_p = 1.0 \times 10^8$ kg/m^{3}s, $\rho_{fw} = 1.0 \times 10^3$ kg/m^3.

From Figure 4, the vertical deformation of the structural beam of the tunnel increases with the increase in riverbed water depth. However, when the water depth of the riverbed increases to a certain value, $h_w = 4.0$ m, the water depth of the riverbed has little impact on the vertical deformation of the beam. With load speed increasing, tunnel structure beam vertical vibration is enhanced, and when the riverbed water depth is larger, even at low speed, the tunnel structure beam vibration fluctuates. The greater the riverbed depth, the more significant the tunnel structure beam vibration, showing that the existence of riverbed water greatly reduces the ray wave speed of fluid-saturated soil bed foundation systems, therefore the speed of high water levels must be controlled.

(a)

(b)
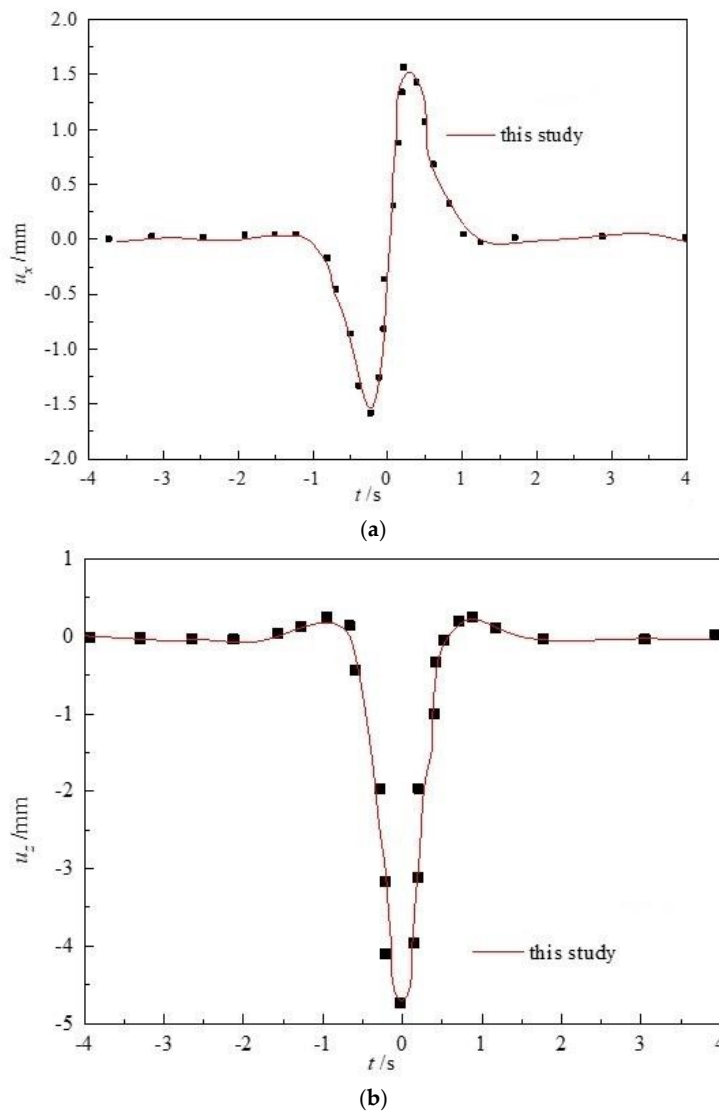
Figure 3. Comparison with reference results. (**a**) horizontal displacement, (**b**) vertical displacement. The black square refers to Ref. [26].

(a)

(b)

(c)

Figure 4. Vertical displacement change of the structural beam of the underwater immersed tunnel during different riverbed water depths. (**a**) $v_c = 0.2\ v_s$, (**b**) $v_c = 0.5\ v_s$, (**c**) $v_c = 1.2\ v_s$.

Figures 5 and 6 show the change in shear force and bending moment of the tunnel structure beam under different riverbed water depth h_w = 0.0 m, 2.0 m, 4.0 m, and 7.0 m. $v_c v_s$ from Figures 5 and 6, the bending moment and shear force of the tunnel structure beam across the river increase with the increase in riverbed water depth. When the load moves at a low speed (<0.5), the bending moment and shear peak of the beam increase as the load speed increases, and when the load speed reaches a high speed, the bending moment and shear decrease as the load speed increases, and the distribution range is relatively narrow. With the increase in movement speed, the load is transferred more to the bed foundation to reduce the internal force of the beam.

Figures 7–9 show the displacement and pore pressure changes of the observation point (A (0, 2.0 m)) in riverbed soil under different riverbed water h_w depths = 0.0 m, 2.0 m, 4.0 m, and 7.0 m.

From Figures 7 and 8, the vertical, horizontal displacement, and hole pressure of the observation point increase as the water depth of the riverbed increases, and the existence of the riverbed water makes the vibration of the observation point more significant, indicating that when the load speed is small, such as v_c = 0.2 v_s, the vertical and horizontal displacement of the temporal dynamic response of the observation point is basically symmetrically distributed on both sides of the moment of load arrival. With increasing load speed and displacement amplitude, the longer the vibration time of the observation point in the riverbed foundation, the more its symmetry about the moment of load arrival disappears. And the phenomenon of shock waves appears. Compared with the vertical and horizontal displacement when the moving load is about to reach the observation point $t < 0$ and when the load leaves the observation point $t > 0$, it shows that when the load is about to reach the observation point $t < 0$, the vibration wave frequency at the surface observation point of the soil is higher. But with a smaller amplitude, Presented as the Doppler effect, that is, when the load approaches the observation point, higher-frequency vibrations will occur. The further the load is away from the observation point, the lower the vibration frequency. But the amplitude of the vibration wave is just opposite to the law of the vibration frequency.

From Figure 9, the hole pressure at the observation point increases with the increase in load velocity. In addition, at low speed (v_c = 0.2 v_s), the pore pressure symmetry appears to point t = 0.0 s. However, at the high speed (v_c = 1.2 v_s), the symmetry disappears (Figure 7c). And there is negative pressure on t = 0.0 s.

Example 3: Influence of the Permeability Coefficient of a Saturated Foundation load speed v_c = 0.2 v_s, h_w = 2.0 m; the calculation parameters of riverbed saturated soil and underwater immersed tunnel beam are the same as in Example 2, investigating the influence of the permeability coefficient of saturated foundation b_p = 1.0×10^5~1.0×10^{11} kg/m^3·s to the displacement, shear, and bending moment of the tunnel structure beam and the displacement and pore pressure of the internal observation point in river bed soil (A (0, 2.0 m)), as shown in Figures 10 and 11.

From Figures 10 and 11, with the increase in the bp value of the saturated foundation (enhanced soil permeability), the vertical displacement, bending moment, shear force of the tunnel structure beam, the vertical and horizontal displacement, and the hole pressure of the observation point increase. However, when the bp value of a saturated foundation increases to a certain value h_w = 4.0 m, it has little influence on the vertical displacement, bending moment, shear force of the beam, vertical and horizontal displacement, and pore pressure of the observation point. The soil with poor permeability produces large pore pressure under the action of a load.

Example 4: Influence of the viscosity coefficient of different viscoelastic beams.

In the case of the viscosity coefficient of different viscoelastic beams: η = 3.0×10^5 Pa, 3.0×10^7 Pa, 3.0×10^9 Pa, 3.0×10^{11} Pa, $E_p^{(1)}$ = $E_p^{(2)}$ = 2.0×10^9 Pa, the load speed v_c = 0.2 v_s, h_w = 2.0 m, the calculation parameters of other saturated riverbed soil are the same as in Example 2. The elastic modulus and viscoelastic coefficient of the viscoelastic beam affect the displacement, shear, and bending moments of the tunnel structure beam and the
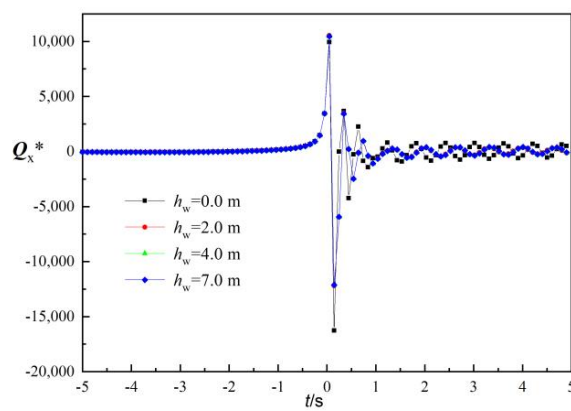
displacement and pore pressure change of the soil internal observation point (A (0, 2.0 m)), as shown in Figures 12 and 13.
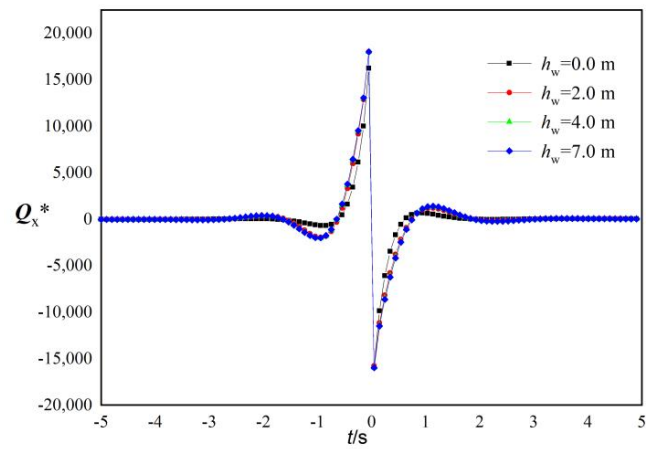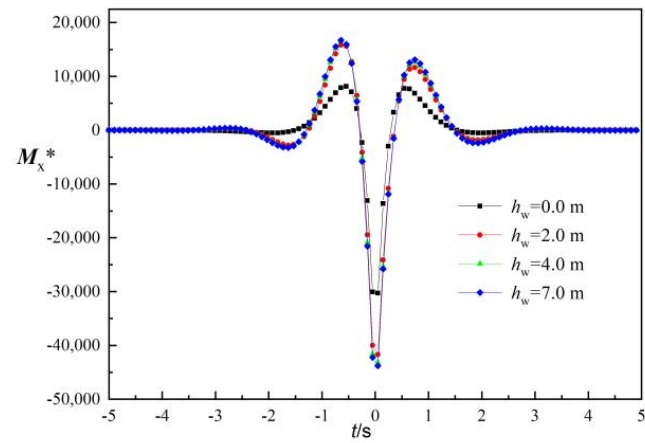

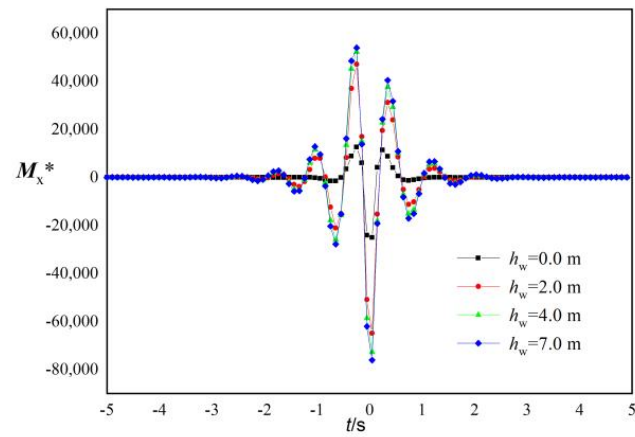(**a**) v$_c$ = 0.2 v_s
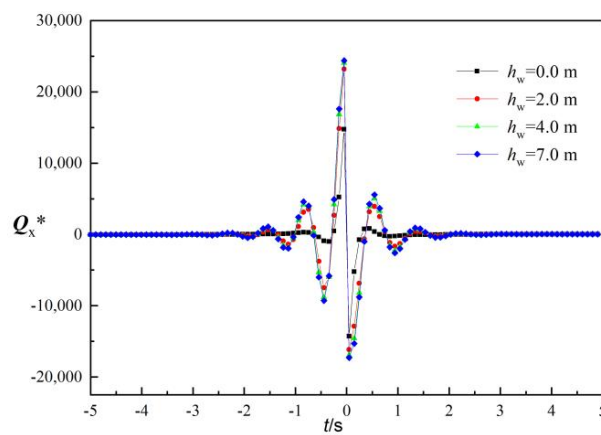
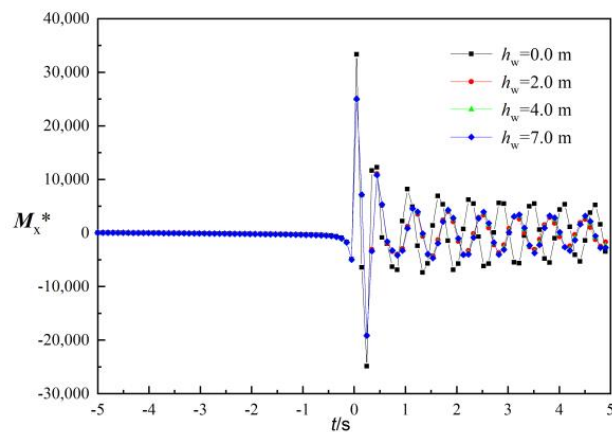(**b**) v$_c$ = 0.5 v_s

(**c**) v$_c$ = 1.2 v_s

Figure 5. Shear force change of the structural beam of the underwater immersed tunnel during different riverbed water depths. (**a**) v$_c$ = 0.2 v_s, (**b**) v$_c$ = 0.5 v_s, (**c**) v$_c$ = 1.2 v_s.
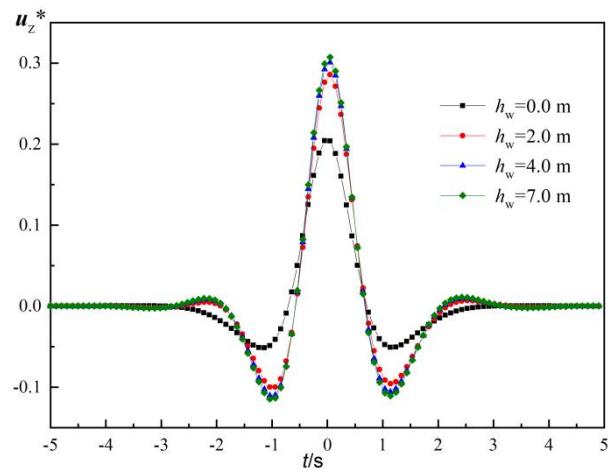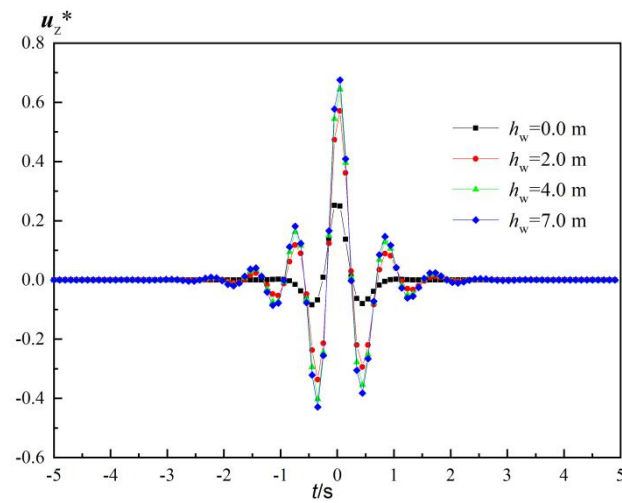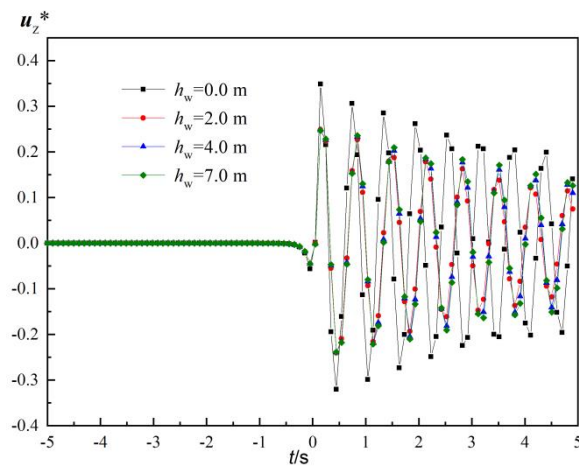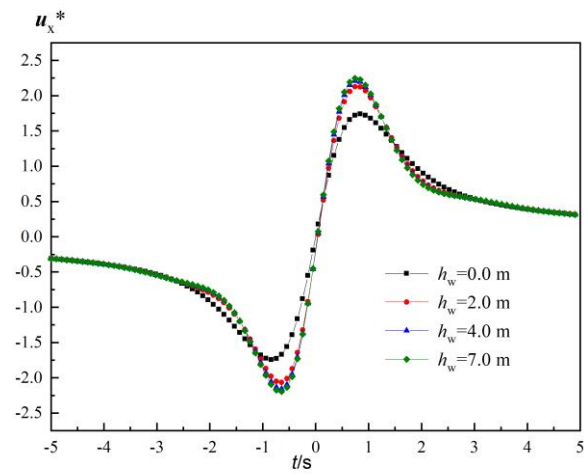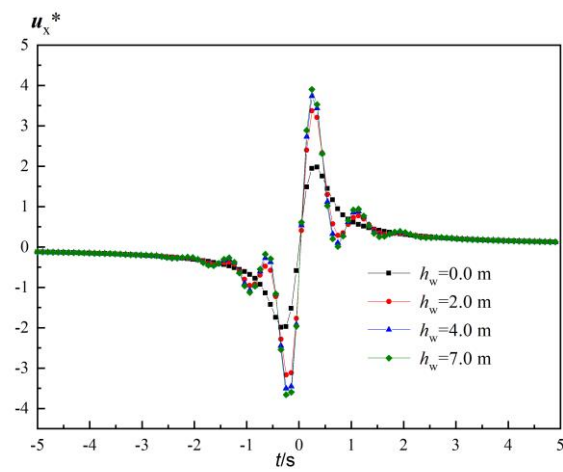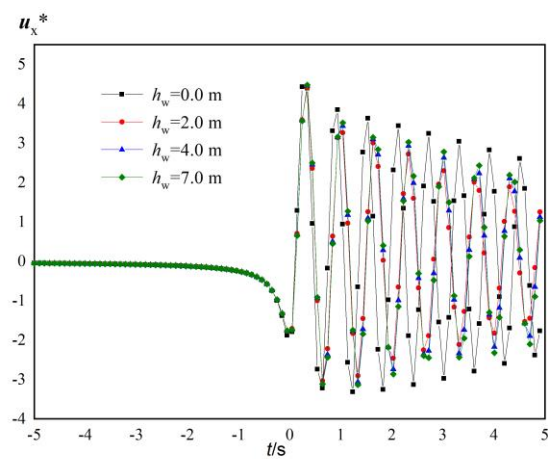
(**a**)

(**b**)

(**c**)

Figure 6. Change of bending moment of the underwater immersed tunnel during different riverbed water depths. (**a**) $v_c = 0.2\ v_s$, (**b**) $v_c = 0.5\ v_s$, (**c**) $v_c = 1.2\ v_s$.

(**a**)

(**b**)

(**c**)

Figure 7. Change of vertical displacement of riverbed foundation observation point during different riverbed water depths. (**a**) $v_c = 0.2\ v_s$, (**b**) $v_c = 0.5\ v_s$, (**c**) $v_c = 1.2\ v_s$.

(**a**)

(**b**)

(**c**)

Figure 8. Horizontal displacement change of riverbed foundation observation point A (0.0 m, 2.0 m) at different riverbed water depths. (**a**) $v_c = 0.2 \, v_s$, (**b**) $v_c = 0.5 \, v_s$, (**c**) $v_c = 1.2 \, v_s$.
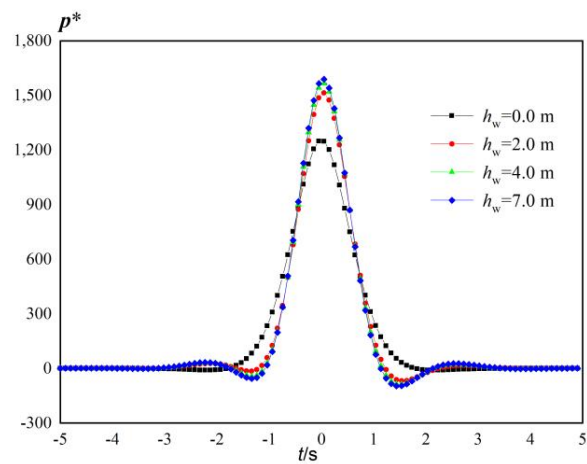
(**a**)
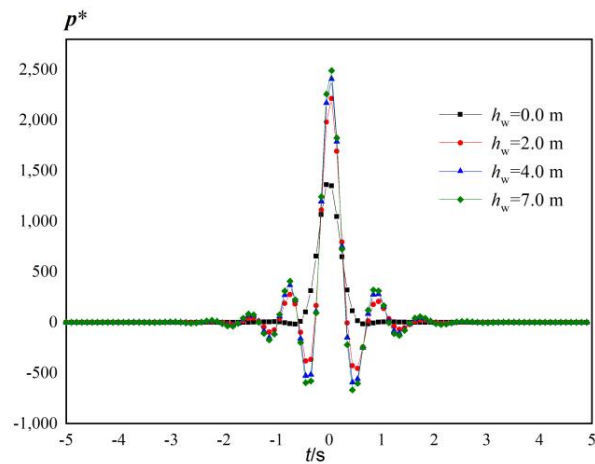
(**b**)
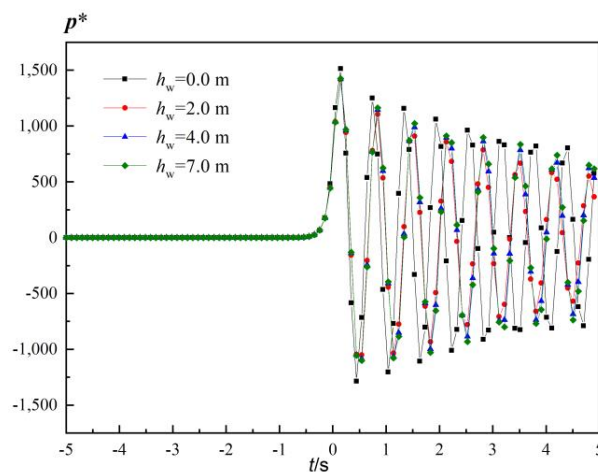
(**c**)

Figure 9. Change of hole pressure at the observation point of the riverbed foundation during different riverbed water depths. (**a**) $v_c = 0.2\ v_s$, (**b**) $v_c = 0.5\ v_s$, (**c**) $v_c = 1.2\ v_s$.
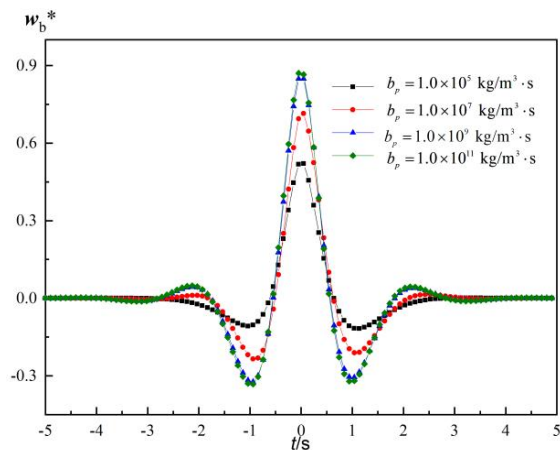
(**a**)
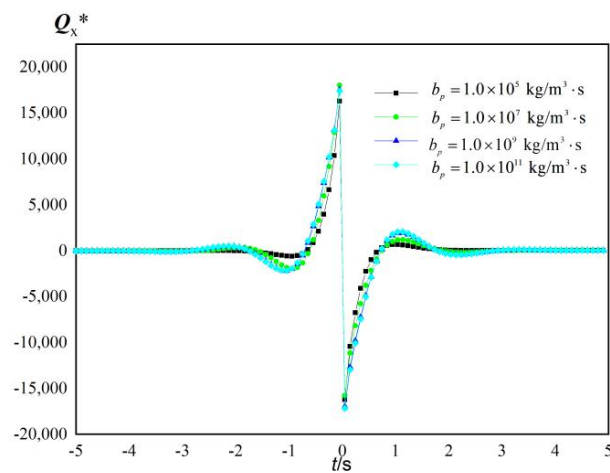
(**b**)
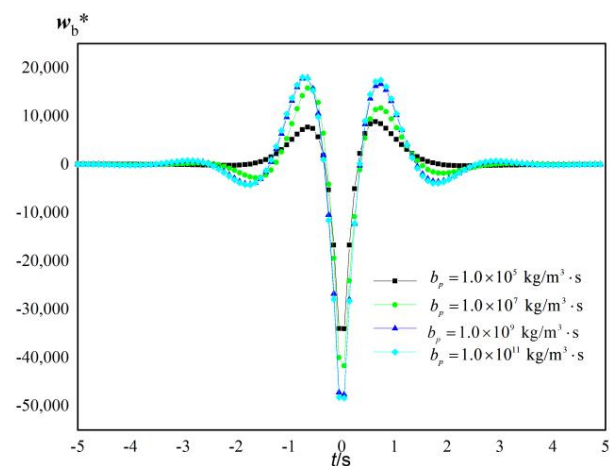
(**c**)

Figure 10. Influence of different riverbed foundation permeability characteristics on the vibration of an underwater immersed tunnel structure beam. (**a**) vertical displacement, (**b**) shear force, (**c**) bending moment.
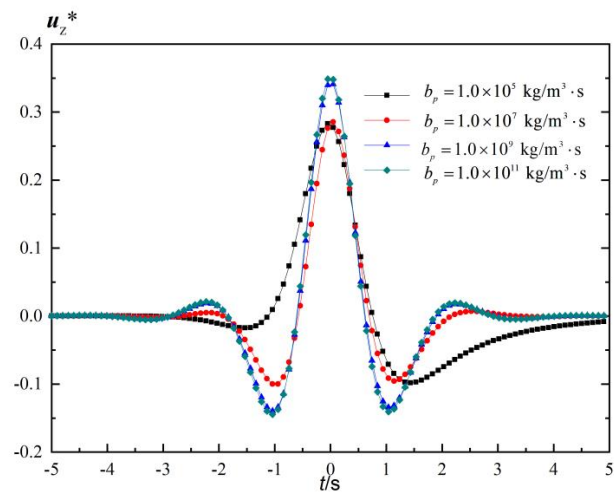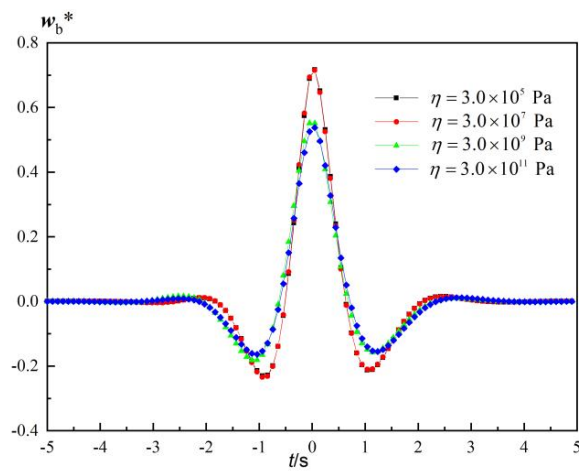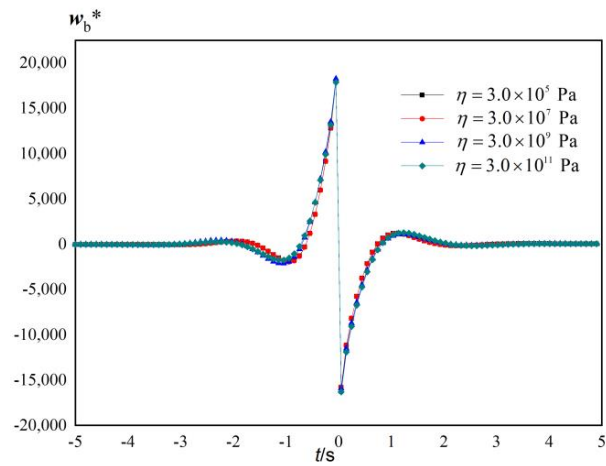
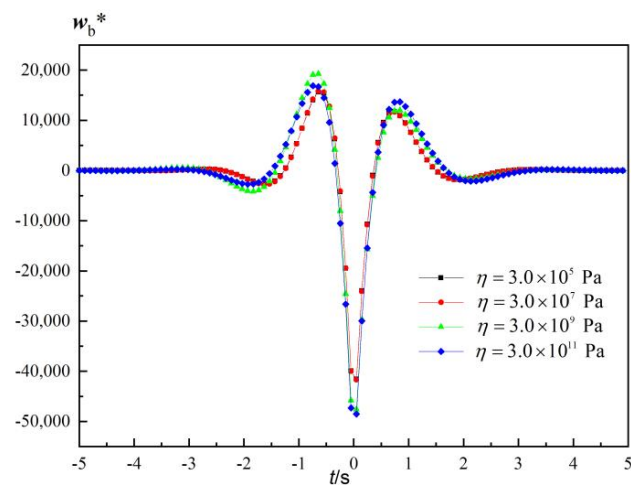(**a**)
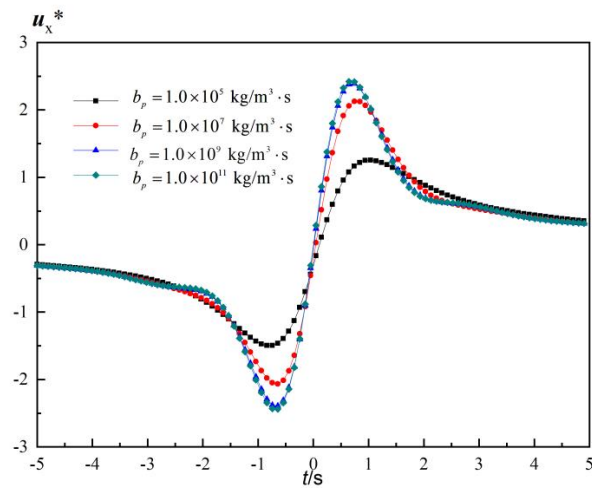
(**b**)
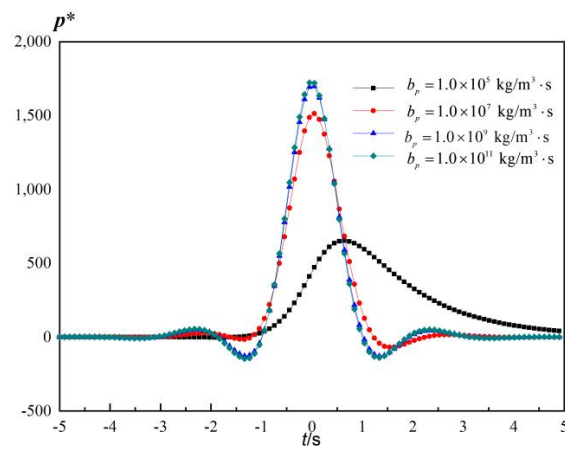
(**c**)

Figure 11. Influence of the permeability characteristics of different riverbed foundations on the vibration of the observation points in the foundation. (**a**) vertical displacement, (**b**) Horizontal displacement, (**c**) Hole pressure.
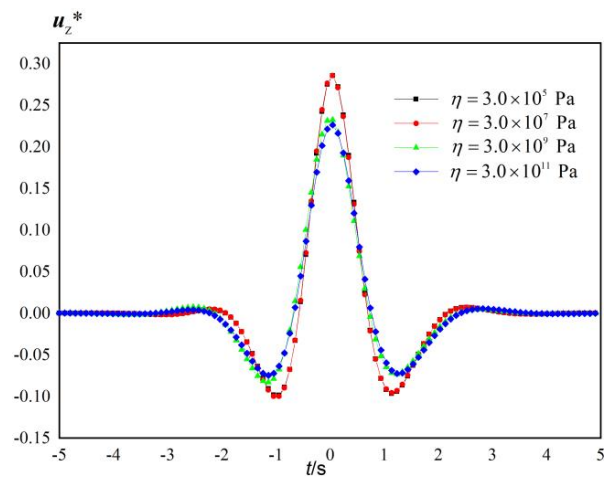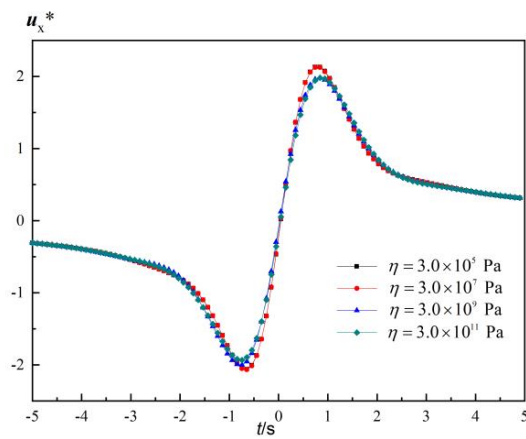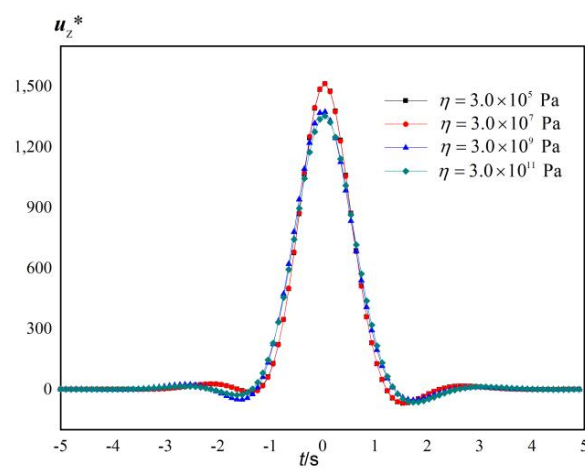
(**a**)

(**b**)

(**c**)

Figure 12. Effect of the viscosity coefficient characteristics of different viscoelastic beams on the vibration of underwater immersed tunnel structure beams. (**a**) vertical displacement, (**b**) shear force, (**c**) bending moment.

(**a**)

(**b**)

(**c**)

Figure 13. Effect of the viscosity coefficient characteristics of different viscoelastic beams on the vibration of the observation points in the foundation. (**a**) vertical displacement, (**b**) Horizontal displacement, (**c**) Hole pressure.

Figures 12 and 13 show that as the viscosity coefficient of the Euler beam of the tunnel structure through the river increases, the vertical displacement, shear force, and vibration amplitude of the bending moment of the beam decrease, but when the viscosity coefficient of the beam increases, such as $\eta = 3.0 \times 10^9$ Pa, which has little influence on the vertical displacement, shear force, and vibration amplitude of the bending moment, it indicates that the elastic modulus of the viscoelastic Euler beam doesn't change with the calculation frequency and shows plasticity. Therefore, the standard solid model of a viscoelastic beam can better describe the creep and relaxation of the material.

5. Conclusions

Based on the theory of ideal fluid and the dynamic behavior of saturated soil, the infinitely long viscoelastic beam model embedded in the fluid-saturated soil system is adopted to analyze the vibration response of the underwater tunnel. The analysis considers different factors such as water depths, load velocities, and viscoelastic beam parameters of the riverbed foundation. The results indicate that:

1. The riverbed depth affects the dynamic response of the tunnel during operation. As the riverbed depth increases, the vertical amplitude of the tunnel structure beam increases. Moreover, when the riverbed depth is significant, even at low speeds, the vibration of the tunnel structure beam becomes fluctuating. This indicates that the riverbed water significantly reduces the Rayleigh wave velocity of the fluid-saturated soil system in the riverbed foundation. Therefore, it is necessary to control the driving speed during high water levels.
2. When the load speed reaches a very high level, the bending moment and shear force of the tunnel structure beam decrease as the load velocity increases. The distribution range is also relatively narrow. As the moving speed increases, more of the load is transferred to the riverbed foundation, thereby reducing the internal forces in the tunnel structure beam.
3. With the enhanced permeability of the saturated riverbed foundation, the vertical displacement, bending moment, and shear force of the tunnel structure beam increase. For riverbed-saturated foundation soils with poor permeability, the operating load of the subway will generate significant pore pressures in the foundation soil.
4. As the viscosity coefficient of the viscoelastic beam increases, the vertical vibration amplitude of the tunnel structure beam will decrease. However, further increasing the viscosity coefficient of the beam will have little effect on its vibration amplitude. Therefore, the standard solid model of the viscoelastic beam can effectively simulate the creep and relaxation phenomena of the material. objectively reflect the working condition of the concrete structure of the tunnel. It can objectively reflect the working conditions of concrete structures in tunnels.

Author Contributions: H.H.: Conceptualization, Software, Writing—original draft; Y.R.: Investigation; X.X.: Writing—review & editing; B.X.: Methodology, Validation. All authors have read and agreed to the published version of the manuscript.

Institutional Review Board Statement: Not applicable.

Informed Consent Statement: Not applicable.

Data Availability Statement: Data is contained within this article.

Conflicts of Interest: The authors declare no conflict of interest.

References

1. Grantz, W.C. Immersed tunnel settlements (Part 2): Case histories. *Tunn. Undergr. Space Technol.* **2001**, *16*, 203–210. [CrossRef]
2. Pan, Y.; Jun, P. Saito Naotake Construction technology of foundation sand pressing method for tube section of Shanghai Outer Ring immersed tunnel. *Mod. Tunn. Technol.* **2004**, *2*, 41–45.
3. Grantz, W.C. Immersed tube tunnel settlements (Part 1): Nature of settlements. *Tunn. Undergr. Space Technol.* **2001**, *16*, 195–201. [CrossRef]
4. Schmidt, B.; Grantz, W.C. Settlements of immersed tunnels. *J. Geotech. Eng. Div.* **1979**, *105*, 1031–1047. [CrossRef]
5. Wu, S.; Zhan, W.; Wang, L. Health monitoring analysis of force deformation during large section tunnel operation period. *J. Zhejiang Univ.* **2013**, *47*, 595–608.
6. Gang, W.; Su, Q. The influence of vehicle load on submarine immersed tunnel in soft soil area. *J. Earthq. Eng.* **2015**, *37*, 94–99.
7. Gao, F.; Guan, B. The impact of train load on the Changjiang River immersed tunnel. *Railw. J.* **2001**, *23*, 117–120.
8. Gang, W.; Zhu, X.; Su, Q. Calculation method and distribution study of the vertical uneven settlement of the immersed tunnel. *Mod. Tunn. Technol.* **2013**, *6*, 58–65.
9. Zhou, Y.; Yang, W.; Yang, L. Analysis of dynamic response characteristics of shield tunnels in water-rich soft strata under train loads. *Chin. J. Rock Mech. Eng.* **2022**, *41*, 1067–1080.
10. Yang, W.; Yang, L.; Liang, Y. Study on the dynamic response characteristics of road-metro tunnels and surrounding soil under train vibration loads. *Chin. J. Rock Mech. Eng.* **2022**, *41*, 1660–1670.
11. Yong, Y.; Shen, Z.; Yu, H. Longitudinal seismic response analysis of immersed tunnel. *Eng. Mech.* **2015**, *32*, 76–83.
12. Hatzigeorgiou, G.D.; Beskos, D.E. Soil-structure interaction effects on seismic inelastic analysis of 3-D tunnels. *Soil Dyn. Earthq. Eng.* **2010**, *30*, 851–861. [CrossRef]
13. Chen, S. *Nonlinear Dynamics Research of Vibration of Viscoelastic Structures*; Guangxi University of Science and Technology: Liuzhou, China, 2015.
14. Gu, M. Investigation of constitutive relation of viscoelatic material. *J. Guilin Inst. Electron. Technol.* **1991**, *1*, 77–85.
15. Liu, C. *Dynamic Modeling and Analysis of Viscoelastic Composite Beams*; Northeastern University: Boston, MA, USA, 2011.
16. Suire, G.; Cederbaum, G. Periodic and chaotic behavior of viscoelastic nonlinear(elastic) bars under harmonic excitations. *Int. J. Mech. Sci.* **1995**, *37*, 753–772. [CrossRef]
17. Argyris, J. Chaotic vibrations of a nonlinear viscoelastic beam. *Chaos Solitons Fractals* **1996**, *7*, 151–163. [CrossRef]
18. Chen, L.; Cheng, C.; Zhang, N. A dynamic model for nonlinear large-defection viscoelastic beams and its simplification. *Shang Hai J. Mech.* **1999**, *3*, 302–305.
19. Chen, L.; Cheng, C. Dynamical behavior of nonlinear viscoelastic beams. *Appl. Math. Mech.* **2000**, *9*, 897–902.
20. Marynowski, K.; Kapitaniak, T. Kelvin-Vogit versus Burgers internal damping in modeling of axially moving viscoelastic. *Int. J. Non-Linear Mech.* **2002**, *37*, 1147–1161. [CrossRef]
21. Li, J.; Liu, H. High precision integration for dynamic response of viscoelastic composite structure. *J. Mach. Des.* **2003**, *10*, 8–9+13.
22. Li, B.; Tang, Y.; Ding, H.; Chen, L.Q. Nonlinear vibrations of axially moving viscoelastic Timoshenko beams under strong external excitation. *J. Vib. Shock* **2012**, *31*, 142–146.
23. Lu, J.F.; Jeng, D.S. Green's function for a harmonic acoustic point source within seawater overlying a saturated poroelastic seabed. *J. Sound Vib.* **2007**, *307*, 172–186. [CrossRef]
24. Biot, M.A. Generalized theory of acoustic propagation in porous dissipative media. *J. Acoust. Soc. Am.* **1962**, *34*, 1254–1264. [CrossRef]
25. Lu, S.; Wei, G. Vibration prediction of immersed tube tunnels under vehicle loads based on Timoshenko beam theory. *Chin. J. Geotech. Eng.* **2018**, *40*, 627–1634.
26. Metrikine, A.V.; Vrouwenvelder, A. Surface ground vibration due to a moving train in a tunnel: Two-dimensional model. *J. Sound Vib.* **2000**, *234*, 43–66. [CrossRef]
27. Nowacki, W. *Theory of Elasticity*; Mir Publishers: Moscow, Russia, 1975. (In Russian)